Comparison of biomechanical models for MRI to X-ray mammography registration

T. Hopp, W. de Barros Rupp Simioni, J.A. Exposito Perez, N.V. Ruiter

Karlsruhe Institute of Technology
Institute for Data Processing and Electronics
Karlsruhe, Germany
torsten.hopp@kit.edu

Abstract. Increasing interest in multimodal breast cancer diagnosis has led to the development of methods for MRI to X-ray mammography registration. The severe breast deformation in X-ray mammography is often tackled by biomechanical models, yet the required complexity of the deformation model and the simulation strategy vary strongly in literature. We present an automated patient-specific biomechanical model based registration method and compare different biomechanical models with isotropic and orthotropic material, with and without estimation of the unloaded breast state. A patient-specific optimization of simulation and preprocessing parameters is proposed. Both the target registration error (TRE) as well as the breast overlap of X-ray mammogram and registered MRI are assessed for four patients. Patient specific optimization decreases the registration error by 40% to approximately 12 mm. Compared to a mere isotropic material model, including the estimation of the unloaded state or applying an orthotropic material improves both the TRE and the overlap of X-ray mammogram and registered MRI.

Keywords: Breast image registration, Biomechanical model, Magnetic Resonance Imaging, X-ray mammography

1 Introduction

Medical imaging is essential for early breast cancer diagnosis. Due to several screening programs around the world, X-ray mammography became the current standard method [1], while additional imaging by e.g. magnetic resonance imaging (MRI) is frequently used in case of suspicious findings. An increasing interest in multimodal diagnosis [2] has led to the development of image registration methods to enable intuitive spatial correlation of three-dimensional MRI volumes and two-dimensional X-ray mammograms. Such an registration poses a challenge as nonlinear deformations occur when the breast is subject to mammographic compression, while the MRI is taken in prone position with the breast mostly pendulous in the MRI coil.

Several approaches including affine transformations [3], spline transformations [4] and biomechanical models [5–8] have been presented to predict the

deformation of the breast. Biomechanical models use simplified geometries [9], homogeneous material [5], more complex patient-specific modeling with respect to inner structures [6, 8] and advanced boundary conditions [7]. Biomechanical models assuming isotropic material are often not able to obtain the patient-specific shape of the breast depicted in the mammogram. To tackle this problem, models, which assume the prone MRI as unloaded state, apply anisotropic materials [6, 9] or post-processing steps [8], while some approaches propose removing the gravity effect from the MRI [10, 11] before applying compression [7].

There has been no conclusive comparison of these strategies yet. In this paper we present our automated and patient-specific biomechanical model generation method, which is an extension to [8]. It was included in a parameterizable framework for comparison and optimization of breast image registrations. We propose a patient-specific optimization of model and processing parameters and present first registration results with in-vivo data. In particular we use a consistent patient collective to compare biomechanical models with anisotropic and isotropic material, as well as with and without estimation of the unloaded state.

2 Methods

The aim of the registration is to bring the breast in the MRI into a configuration which is comparable to the breast shape in X-ray mammography. The deformation applied to the MRI is controlled by a deformation model, which in our approach is based on biomechanical simulation of the mammographic breast deformation by applying compression plates (Fig. 1).

2.1 Automated biomechanical model generation

To obtain the patient-specific breast geometry, the MR volume is segmented into background, fatty tissue, glandular tissue and breast muscle. We first separate the breast from the background using a two-class Fuzzy-C-means clustering (FCM). Afterwards the MR volume is divided at the sternum into a dorsal and ventral part. In the ventral part fatty and glandular tissue are segmented by a two-class FCM similar to [12], while in the dorsal part, a three-class FCM is applied. To correct for outliers due to MRI field inhomogeneities, the breast muscle is detected slicewise by thresholding the directional gradient of the image after applying an anisotropic diffusion filter. Ventral and dorsal segmentations are combined and the tissue classes with maximum likelihood are used as final segmentation. According to the segmented tissue type, voxels are assigned an X-ray attenuation coefficient based on literature values [13].

The MRI volume is clipped in dorsal direction at the position cut_z for which the volume of the breast tissue in the MRI fits best the estimation of the imaged tissue volume in the X-ray mammograms per our previously described method [8]. Afterwards MRI and X-ray mammogram are initially aligned at their centers of mass. A rotation around the vendral-dorsal axis (rot_z) can be applied to compensate for uncertainties in the mammographic projection angle and manual

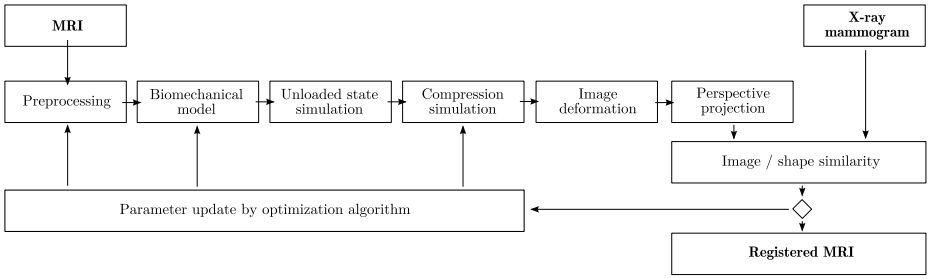

Fig. 1. Overview of the processing steps and optimization loop of the registration.

positioning of the breast on the mammographic compression plates. The MRI is additionally rotated around the cranio-caudal axis (rot_y) to meet the mammography guidelines, which suggest a tilting of the patient by approximately 5° to the not imaged side [14].

To create the model geometry, a tetrahedral meshing algorithm [15] based on Delaunay triangulation converts the segmented MRI volume into approximately 1000-2000 4-node elements. At tissue interfaces, the algorithm is allowed to reduce the volume of the elements to reflect the surfaces. Though the limited number of elements may not accurately reflect tissue interfaces, this tradeoff was made to reduce the computational expense. A layer of membrane elements with adjustable thickness is added on top of the breast surface elements to model skin. Nodes at the back of the model are fixed in ventral-dorsal direction as suspension at the chest. For the compression simulation, acrylic glass plates consisting of 8-node hexahedrons are added to the model. A small-sliding interface with adjustable friction between plate and breast surface is defined.

Two material models are implemented: an isotropic hyperelastic neo-hookean material (*iso*) [16] and an hyperelastic fung orthotropic material (*ortho*) [17]. While isotropic material deforms uniformly in all directions of space, an orthotropic material can deform non-uniformly, e.g. in one preferred direction. The *iso* material is defined by two material constants C_{01} and D_1 which are determined by a Young's modulus E and a Poisson ratio ν_i as $C_{01}=\frac{E}{4(1+\nu_i)}$ and $D_1=\frac{2}{3E(1-3\nu_i)}$. A constant ν_i of 0.495, within the range used in literature (e.g. [6]), is applied to model nearly incompressible material. While the *iso* material only depends on scalar parameters, the *ortho* material has three Young's moduli E_1, E_2 and E_3 and six Poisson's ratios ν_{jk} with $j,k \in [1,2,3]\,, j \neq k$. E_j expresses the stiffness of the material under a load in direction j, while ν_{jk} expresses the contraction in k under a load in direction j. Following [18], assuming a decoupling of normal and shear components, E_k, ν_{jk} and the shear moduli μ_{jk} form the elasticity tensor $\mathbf{C}$ as described in eq. 1.

$$\mathbf{c}^{-1}=\begin{bmatrix} \frac{1}{E_1} & -\frac{\nu_{21}}{E_2} & -\frac{\nu_{31}}{E_3} & 0 & 0 & 0 \\ -\frac{\nu_{12}}{E_1} & \frac{1}{E_2} & -\frac{\nu_{32}}{E_3} & 0 & 0 & 0 \\ -\frac{\nu_{13}}{E_1} & -\frac{\nu_{23}}{E_2} & \frac{1}{E_3} & 0 & 0 & 0 \\ 0 & 0 & 0 & \frac{1}{\mu_{12}} & 0 & 0 \\ 0 & 0 & 0 & 0 & \frac{1}{\mu_{23}} & 0 \\ 0 & 0 & 0 & 0 & 0 & \frac{1}{\mu_{31}} \end{bmatrix} \quad (1)$$

To obtain a stable solution ν_{jk} are calculated from a single parameter $\nu_o \in [-1, ½]$ as $\nu_{jk} = \nu_o \sqrt{E_j E_k^{-1}}$ [18]. Accordingly, μ_{jk} is calculated from E_j and ν_o as $\mu_{j,k} = ½(E_j + E_k)(2(1+\nu_o))^{-1}$ [18] resulting in four free parameters for the *ortho* material. The material parameters of *iso* and *ortho* material are chosen independently for all segmented tissue types.

The estimation of the unloaded state follows an inversion of the gravity by applying a body load with an acceleration of $g = 9.81 m/s$ in dorsal direction due to its computational benefit and comparable accuracy with more complex methods [19]. To simulate the mammographic compression, the compression plates are moved to the distance d_p expressing the compression thickness, which is initially given by the mammogram's meta data. The biomechanical simulations are formulated with the Finite Element Method (FEM) and computed using the dynamic FE solver for large deformations of the software package ABAQUS [20] in a quasi-static configuration.

After the FEM simulation, the deformation is applied to the MRI volume by linear interpolation of the deformation within the 4-node tetrahedrons and tri-linear interpolation of intensity values. To render an image comparable to the mammogram, a perspective ray casting is carried out. The assigned X-ray attenuation coefficients are used to compute the log-transformed intensity at each detector pixel.

2.2 Patient-specific optimization

To adapt the image registration to patient-specific conditions and overcome uncertainties like the mammographic projection angle or the tissue volume estimation, an image based optimization is applied. Simulated annealing optimization [21] with a maximum number of iterations as stopping criterion is used. The optimization criterion can be any metric to judge the image respectively shape similarity. In this study we used the overlap of the mammogram with the projection of the deformed MRI volume, expressed by the Dice coefficient Dice_B [22] as optimization criterion. The parameters rot_z, rot_y, d_p, cut_z are optimized simultaneously with the material parameters. In case of the *iso* material, these include the Young's modulus for fat (E_{fat}) and glandular tissue (E_{gland}), in case of the *ortho* material, E_1, E_2, E_3 and ν_o of fat and glandular tissue.

2.3 Evaluation method

For evaluation of the registration accuracy, clinical routine examinations were used, each consisting of T1-weighted MRI volumes and corresponding cranio-

caudal (CC) mammograms. They were selected to include at least one lesion, which was clearly visible in both modalities. Those lesions were used as landmarks, which serve as ground truth for calculating the target registration error (TRE) as the Euclidean distance between the mammogragphy marking and the MRI marking after deformation and projection. Additionally Dice_B, which also acts as optimization criterion, is given to estimate the overlap enhancement by the patient-specific optimization. For a proof of principle, four datasets were included in this study.

3 Results

The registration was computed with different configurations of the deformation model and degrees of freedom of the model parameters as summarized in Table 3. In the four datasets a total of eight lesion annotations were available. Compared to an unoptimized registration, optimizing the cut_z parameter already improves the average TRE and partly Dice_B. This demonstrates the need for a sophisticated tissue estimation in both images.

A considerable improvement of the average overlap can be identified by including an estimation of the unloaded state (*unload* = yes) in the *iso* material model or using the *ortho* material model. Both strategies deliver comparable results and are able to reduce the average TRE to approximately $12\,mm$ while increasing Dice_B close to the ideal value of 1. A comparison of mammograms and registered MRIs is given in Figure 2.

Material	**Optimized parameters**	**Unload**	$\overline{\textbf{TRE}}$	$\overline{\textbf{DICE}_B}$
iso	—	no	24.1 mm	0.853
	cut_z	no	14.4 mm	0.908
	E_{fat}, E_{gland}, cut_z, rot_z, rot_y, d_p	yes	12.1 mm	0.975
ortho	E_1, E_2, E_3 and ν_o for fat and glandular tissue, cut_z, rot_z, rot_y, d_p	no	12.7 mm	0.969

Table 1. Summary of registration results using different material models and optimization options.

4 Discussion and Conclusion

The presented image registration framework enables new possibilities in investigating and comparing material models, registration strategies and patient-specific optimization for registration of X-ray mammograms with MRI. We considerably extended our previous biomechanical model [8] by a state of the art segmentation algorithm, including muscle and skin, an X-ray like ray casting projection, estimation of the unloaded state and orthotropic material. Our preliminary results with a limited number of datasets show that both strategies applied in literature (anisotropic material, estimating the unloaded state) are

able to enhance the registration results compared to a mere isotropic model. This potentially enables to omit post-processing deformations applied in our previous work [8] and increase the registration accuracy. For a proof of principle, CC view mammograms were used in this study. In future we will apply the framework to an extend patient collective and oblique mammographic views to investigate the influence of registration and preprocessing parameters more deeply.

The obtained results were achieved with a fixed number of 100 iterations as stopping condition, which was applied for all experiments. Registration with optimization of a larger number of parameters simultaneously might be enhanced by a higher number of iterations. As optimization criterion the Dice coefficient was applied, which judges the shape similarity of X-ray mammogram and projection of MRI independently from the presence of inner structures or abnormalities. The computationally most expensive biomechanical simulation with ABAQUS is the current bottleneck. Integrating dedicated GPU-accelerated FEM solvers in future will enable a faster computation per iteration and thereby possibly allow for the optimization with even more patient-specific parameters. Furthermore the optimization method and its parameterization have an influence on the outcome. We are currently investigating the influence of these.

Despite these limitations, the results of the registration are promising as with both proposed biomechanical models, the overlap of the X-ray mammogram and the projection of the MRI can be considerably enhanced from an average Dice coefficient of 0.91 to approximately 0.97 and 0.98 respectively. The overall registration accuracy is in the same range as our previous method [8], however not any longer using a post-processing step.

References

[1] E. Altobelli, L. Lattanzi: Breast cancer in European Union: An update of screening programmes as of March 2014 (Review), Int. J. of Oncology 45: 1785–1792, 2014

[2] C.M.C. Tempany, J. Jayender, T. Kapur, R. Bueno, A. Golby, N. Agar, F.A. Jolesz: Multimodal Imaging for Improved Diagnosis and Treatment of Cancers, Cancer 121: 817–827, 2015

[3] T. Mertzanidou, J. Hipwell, M. J. Cardoso, X. Zhang, C. Tanner, S. Ourselin, U. Bick, H. Huisman, N. Karssemeijer, D. Hawkes: MRI to X-ray mammography registration using a volume-preserving affine transformation, Medical Image Analysis 16(5):966–975, 2012

[4] J. Krüger, J. Ehrhardt, A. Bischof, H. Handels: Simulation of Mammographic Breast Compression in 3D MR Images Using ICP-Based B-Spline Deformation for Multimodality Breast Cancer Diagnosis, Int. J. of Computer Assisted Radiology and Surgery 9(3):367–377, 2014

[5] N.V. Ruiter, R. Stotzka, T.O. Müller, H. Gemmeke, J.R. Reichenbach, W.A. Kaiser: Model-based registration of X-ray mammograms and MR images of the female breast, IEEE Trans. on Nuclear Science 53(1):204–211, 2006

[6] T. Mertzanidou, J. Hipwell, S. Johnsen, L. Han, B. Eiben, Z. Taylor, S. Ourselin, H. Huisman, R. Mann, U. Bick, N. Karsse-meijer, D. Hawkes: MRI to X-ray mammography intensity-based registration with simultaneous optimisation of pose and

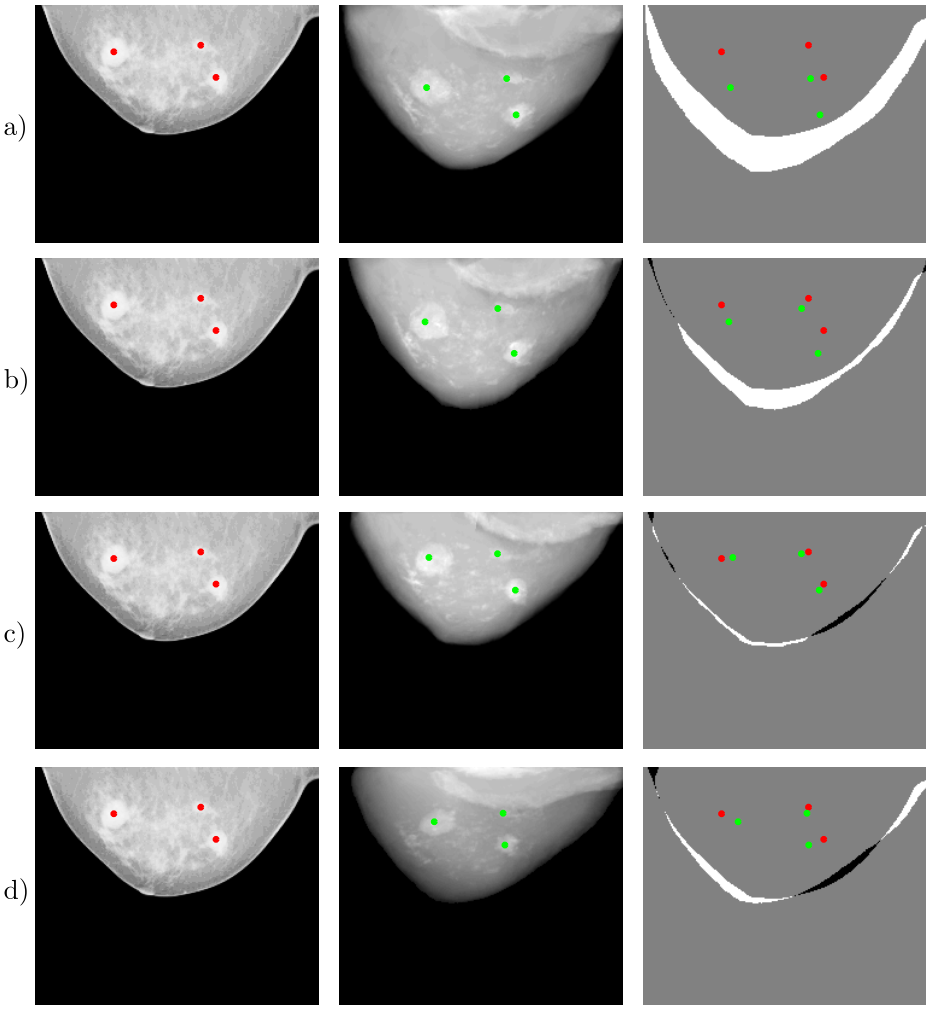

Fig. 2. Comparison of X-ray mammogram (left) and projection of deformed MRI volume (middle) for one patient with three marked lesions. The right images express the overlap of both images by subtracting the binary area of X-ray mammogram and the projection of deformed MRI volume. a) Isotropic model without unloaded state estimation and optimization, b) isotropic model without unloaded state estimation and with optimization of cut_z, c) isotropic model with unloaded state estimation and optimization of all six parameters, d) orthotropic model without unloaded state estimation and with optimization of all 12 parameters. The red dots depict the lesion annotations in the mammogram, the green dots the lesion annotations in the MRI volume after deformation and projection.

biomechanical transformation parameters, Medical Image Analysis 18(4): 674–683, 2014
[7] A.W.C. Lee, V. Rajagopal, T.P. Bararenda Gamage, A.J. Doyle, P.M.F. Nielsen, M.P. Nash: Breast lesion co-localisation between X-ray and MR images using finite element modeling, Medical Image Analysis 17(8):1256–1264, 2013
[8] T. Hopp, M. Dietzel, P.A. Baltzer, P. Kreisel, W.A. Kaiser, H. Gemmeke, N.V. Ruiter: Automatic multimodal 2D/3D breast image registration using biomechanical FEM models and intensity-based optimization, Medical Image Analysis 17(2): 209–218, 2013
[9] T. Mertzanidou, J. Hipwell, L. Han, H. Huisman, N. Karssemaijer, and D. Hawkes, MRI to X-ray Mammography Registration Using an Ellipsoidal Breast Model and Biomechanically Simulated Compressions,"' in Proc. of the Workshop on Breast Image Analysis, MICCAI 2011, pp. 161–168, 2011.
[9] C. Tanner, M. White, S. Guarino, M. Hall-Craggs, M. Douek, D. Hawkes: Anisotropic Behaviour of Breast Tissue for Large Compressions, Proc. IEEE Int. Symp. on Biomedical Imaging: From Nano to Macro: 1223–1226, 2009
[10] V. Rajagopal, J.H. Chung, D. Bullivant, P.M.F. Nielsen, M.P. Nash: Determining the finite elasticity reference state from a loaded configuration, Int. J. for Numerical Methods in Engineering 72(12): 1434–1451, 2007
[11] T. Carter, C. Tanner, N. Beechey-Newman, D. Barratt, D. Hawkes: MR navigated breast surgery: Method and initial clinical experience, Medical Image Computing and Computer Assisted Intervention (MICCAI), LNCS 5242:356–363, 2008
[12] S. Wu, S. Weinstein, B.M. Keller, E.F. Conant, D. Kontos: Fully-Automated Fibroglandular Tissue Segmentation in Breast MRI, in Proc. IWDM 2012, LNCS 7361, pp. 244—251, 2012
[13] K. Bliznakova, Z. Bliznakova, V. Bravou, Z. Kolitsi, N. Pallikarakis: A three-dimensional breast software phantom for mammography simulation, Physics in Medicine and Biology 48: 3699–3719, 2003
[14] V.F. Duda, R. Schulz-Wendtland: Mammadiagnostik, Springer Berlin, 2004
[15] Q. Fang, D. Boas: Tetrahedral mesh generation from volumetric binary and gray-scale images, Proc. of IEEE Int. Symp. on Biomedical Imaging 2009, 1142–1145, 2009
[16] R.S. Rivlin: Large Elastic Deformations of Isotropic Materials. I. Fundamental Concepts, Philosophical Transactions of the Royal Society of London. Series A, Mathematical and Physical Sciences 240(822) , 459–490, 1948
[17] J.D. Humphrey: Mechanics of the Arterial Wall: Review and Directions, Critical Reviews in Biomedical Engineering. 23(1–2):1–162, 1995
[18] Y. Li, J. Barbic: Stable orthotropic materials, Eurographics/ACM SIGGRAPH Symp. on Computer Animation, 2014
[19] B. Eiben, V. Vavourakis, J. Hipwell, S. Kabus, C. Lorenz, T. Buelow, D. Hawkes: Breast deformation modelling: comparison of methods to obtain a patient specific unloaded configuration, in Proc. SPIE Medical Imaging, 9036, 903615, 2014
[20] Dassault Systemes: ABAQUS/CAE 6.13 User's Manual, Online Documentation
[21] S. Kirkpatrick, C.D. Gelatt, M.P. Vecchi: Optimization by Simulated Annealing, Science 220(4598), 671–680 (1983).
[22] L.R. Dice: Measures of the Amount of Ecologic Association Between Species, Ecology 26 (3): 297–302, 1945